Self-organization in purely viscous non-Newtonian turbulence

H. J. Seybold,[1] H. A. Carmona,[2] H. J. Herrmann,[2,3] and J. S. Andrade, Jr.[2,*]
[1]*Physics of Environmental Systems, D-USYS, ETH Zürich, 8093 Zürich, Switzerland*
[2]*Departamento de Física, Universidade Federal do Ceará, Campus do Pici, 60451-970 Fortaleza, Ceará, Brazil*
[3]*PMMH, ESPCI, CNRS UMR 7636, 7 quai St. Bernard, 75005 Paris, France*

(Received 27 April 2018; published 6 June 2019)

We investigate through direct numerical simulations (DNSs) the statistical properties of turbulent flows in the inertial subrange for non-Newtonian power-law fluids. The structural invariance found for the vortex size distribution is achieved through a self-organized mechanism at the microscopic scale of the turbulent motion that adjusts, according to the rheological properties of the fluid, the ratio between the viscous dissipations inside and outside the vortices. Moreover, the deviations from the K41 theory of the structure functions' exponents reveal that the anomalous scaling exhibits a systematic nonuniversal behavior with respect to the rheological properties of the fluids.

DOI: 10.1103/PhysRevFluids.4.064604

I. INTRODUCTION

In many situations ranging from blood flow [1,2] to atomization of slurries in industrial processing [3], one encounters non-Newtonian fluids in turbulent conditions. The first experiments on turbulence in non-Newtonian fluids were already performed in 1931 by Forrest and Grierson [4]. Later, Toms [5] reported experimental results on turbulent flow of linear polymers, and Dogde [6] investigated, both theoretically and experimentally, polymeric gels and solid-liquid suspensions under turbulent-flow conditions. Since then, most theoretical studies have focused on drag reduction [7,8], and the mathematical modeling of wall stresses and boundary layers [9–11]. For isotropic turbulence in dilute polymer solutions, De Angelis *et al.* [12] found through DNS that relaxation connecting different scales significantly alters the energy cascade.

Intuitively, in the inertial subrange, molecular stresses should have a negligible influence on the motion and size of the eddies, regardless of the rheological nature of the fluid [13]. More precisely, even if a more complex constitutive law than a linear one is necessary to describe the stress-strain relation of a moving fluid, one should expect the statistical results obtained for the structure of Newtonian turbulence at the inertial subrange to remain valid. A relevant question that naturally arises is how the local rheological properties of the fluid must rearrange in space and time to comply with this alleged structural invariance. Here we provide an answer for this question by investigating through DNS the statistical properties of coherent structures of Newtonian and non-Newtonian turbulent flows in terms of distributions of vortices sizes. The deviations from the K41 theory in the behavior of these turbulent systems are also studied through the anomalous scaling of their structure functions [14].

*Corresponding author: soares@fisica.ufc.br

II. NUMERICAL SIMULATIONS

For our numerical analysis, we consider a cubic box containing a non-Newtonian fluid and subjected to periodic boundary conditions in all three directions. The mathematical formulation of the fluid mechanics is based on the assumptions that we have an incompressible fluid flowing under isothermal conditions, for which the momentum and mass conservation equations reduce to

$$\rho\frac{\partial \boldsymbol{u}}{\partial t} + \rho\boldsymbol{u}\cdot\nabla\boldsymbol{u} = -\nabla p + \nabla\cdot\boldsymbol{T} + \boldsymbol{\Gamma}, \tag{1}$$

and

$$\nabla\cdot\boldsymbol{u} = 0, \tag{2}$$

where $\boldsymbol{u}$ and p are the velocity and pressure fields, respectively, $\boldsymbol{\Gamma}$ is a forcing term and $\boldsymbol{T}$ is the deviatoric stress tensor given by

$$\boldsymbol{T} = 2\,\mu(\dot{\gamma})\,\boldsymbol{E}, \tag{3}$$

where $\boldsymbol{E} = (\nabla\boldsymbol{u} + \nabla\boldsymbol{u}^T)/2$ is the strain rate tensor and $\dot{\gamma} = \sqrt{2\boldsymbol{E}:\boldsymbol{E}}$ its second principal invariant. The function $\mu(\dot{\gamma})$ defines the constitutive relation, which for a cross-power-law fluid is given by

$$\mu(\dot{\gamma}) = K\dot{\gamma}^{(n-1)}, \quad \mu_1 \leqslant \mu \leqslant \mu_2. \tag{4}$$

The constants μ_1 and μ_2 are the lower and upper cutoffs, respectively, K is called the consistency index, and n is the rheological exponent. The cutoff values, $\mu_1/\mu_N = 10^{-8}$ and $\mu_2/\mu_N = 10^3$, where μ_N is the viscosity of the Newtonian fluid, have been chosen to be sufficiently low in the case of μ_1 and sufficiently high in the case of μ_2 to guarantee that the power-law behavior prevails all over the system, at any time, and for all values of the rheological exponent n. Moreover, the minimum value obtained for the local strain rate in all cases, $\dot{\gamma}_{\min} = 0.5/\tau$ for $n = 0.33$, is comparable to the minimum found for the Newtonian fluid ($n = 1$); namely, $\dot{\gamma}_{\min} = 0.6/\tau$, which are both sufficiently higher than the physical limit that characterizes a slow flow regime. Fluids with $n>1$ are shear-thickening, while shear-thinning behavior corresponds to $n<1$. For $n = 1$, we recover a Newtonian fluid.

A central assumption involved in the theoretical construct of the K41 theory [15–17] is that the fluid flow at a sufficiently large Reynolds is in a homogeneous and locally isotropic state—the so-called fully developed turbulence—that can be described in terms of universal statistical properties [14]. To attain a fully developed turbulent regime, here the fluid is driven by a linear force [18,19]

$$\boldsymbol{\Gamma} = \rho(\boldsymbol{u} - \langle\boldsymbol{u}\rangle)/\tau, \tag{5}$$

where $\langle\boldsymbol{u}\rangle$ is the spatial average of the velocity field and the parameter τ corresponds to a prescribed turnover timescale [19]. Differently from typical schemes, where low-wave-number forcing is numerically applied in Fourier space, the linear forcing method is directly formulated in physical space and can therefore be readily integrated into physical-space numerical solvers [19].

For a given set of turbulent-flow conditions and constitutive parameters of the non-Newtonian fluid, the numerical solution of Eqs. (1) and (2) for the time evolution of the local velocity and pressure fields is obtained through the open source DNS code GERRIS [20]. This code is based on a second-order finite-volume scheme applied to an adaptively refined octree mesh. The maximal refinement level was set to eight subdivision steps, corresponding to a 256-cube discretization of our triple periodic box. This grid refinement technique has been successfully tested and validated for isotropic Newtonian turbulence. More specifically, a test case in which the adaptively refined results are extensively compared with a standard spectral DNS code for the Newtonian case is available in Ref. [21]. Finally, all simulations have been performed by using an unstable Arnold– Beltrami–Childress (ABC) flow as initial configuration [22].

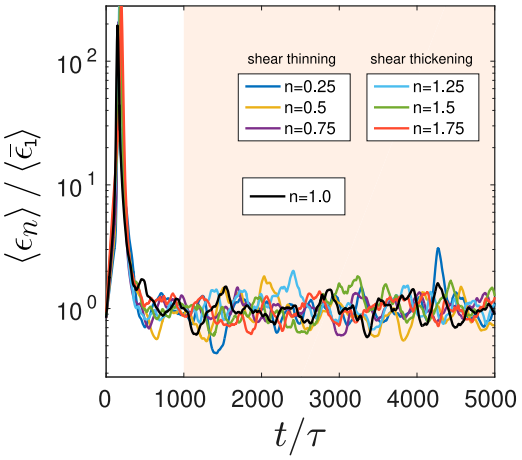

FIG. 1. Normalized dissipated energy as a function of time for different values of n. In all cases, after shooting up, the dissipated energies for distinct values of n drop quickly to eventually reach approximately the same stationary state. The normalization factor, $\langle \bar{\epsilon}_1 \rangle$, corresponds to the average in space and time of the local dissipated energy for the Newtonian fluid ($n = 1$). The average in time is computed at the stationary state, precisely, for $t/\tau > 1000$ (region colored in cream).

III. RESULTS AND DISCUSSION

In Fig. 1 we show the variation in time of the normalized dissipated energy $\langle \epsilon_n \rangle / \langle \bar{\epsilon}_1 \rangle$ in the turbulent system for different values of n, where $\langle \epsilon_n \rangle$ is the average in space of the local rate of dissipated energy per unit of mass $\epsilon_n(\dot{\gamma}) = \nu(\dot{\gamma})\dot{\gamma}^2$ [23,24], with $\nu(\dot{\gamma}) = \mu(\dot{\gamma})/\rho$, for a given value of n, and $\langle \bar{\epsilon}_1 \rangle$ is the average in space and time of the local rate of dissipated energy per unit of mass for the Newtonian fluid ($n = 1$) and for values of time taken over the stationary state. As can be seen, this last condition is ensured here by averaging in time only when $t/\tau > 1000$ for any value of n (region colored in cream in Fig. 1). Throughout this paper the brackets $\langle\ \rangle$ indicate spatial averaging, and temporal averages are denoted with an overbar. Here, we define the Taylor Reynolds number as $\mathrm{Re}_\lambda = \langle v' \rangle_{\mathrm{rms}} \lambda / \langle \nu \rangle$, where $\langle v' \rangle_{\mathrm{rms}}$ is the root mean square velocity, $\lambda = \sqrt{15 \langle \nu \rangle / \langle \bar{\epsilon}_n \rangle} \langle v' \rangle_{\mathrm{rms}}$ is the Taylor microscale. For the Newtonian case, $\mathrm{Re}_\lambda = 75$, and the results of our numerical simulations are quantitatively compatible with those reported by Rosales and Meneveau [19], obtained under the same set of conditions. For non-Newtonian fluid flows, we obtained similar values; namely, $\mathrm{Re}_\lambda = 78$, 79, 77, 72, 78, and 80, for $n = 0.33$, 0.5, 0.75, 1.25, 1.5, and 1.75, respectively.

For comparison, we have performed simulations at higher Reynolds number; namely, $\mathrm{Re}_\lambda = 171$ for the shear-thinning fluid with $n = 0.5$, $\mathrm{Re}_\lambda = 160$ for the Newtonian fluid ($n = 1.0$), and $\mathrm{Re}_\lambda = 151$ for the shear-thickening fluid with $n = 1.5$. The energy spectra for the lower and higher values of Re_λ cases, for the shear-thinning, $n = 0.5$, Newtonian, $n = 1.0$, and shear-thickening, $n = 1.5$, fluids are portrayed in Fig. 2. The spectra (multiplied by $k^{5/3}$) display the same behavior over a large range of wave numbers. Expectedly, we observe the presence of an extended plateau at lower wave numbers for higher Reynolds numbers.

At each time step, the geometric structure of turbulent eddies is characterized in terms of the λ_2-*vortex-criterion* [25], which identifies vortices by the existence of a local pressure minimum, removing the effects of unsteady straining and viscosity. More precisely, the λ_2 *criterion* delimits a vortex boundary based on the value of the second eigenvalue of the tensor, $\boldsymbol{M} = \boldsymbol{E}^2 + \boldsymbol{Q}^2$, where $\boldsymbol{Q} = (\nabla \boldsymbol{u} - \nabla \boldsymbol{u}^T)/2$. Since $\boldsymbol{M}$ is symmetric, it has only real eigenvalues which can be ordered, $\lambda_1 < \lambda_2 < \lambda_3$. Accordingly, a vortex is defined as a connected region in space with at least two negative eigenvalues of $\boldsymbol{M}$, thus leading to the criterion [25] $\lambda_2 < 0$. In practical terms, considering a turbulent system with multiple vortices, we use this definition to identify them as clusters of cells in the

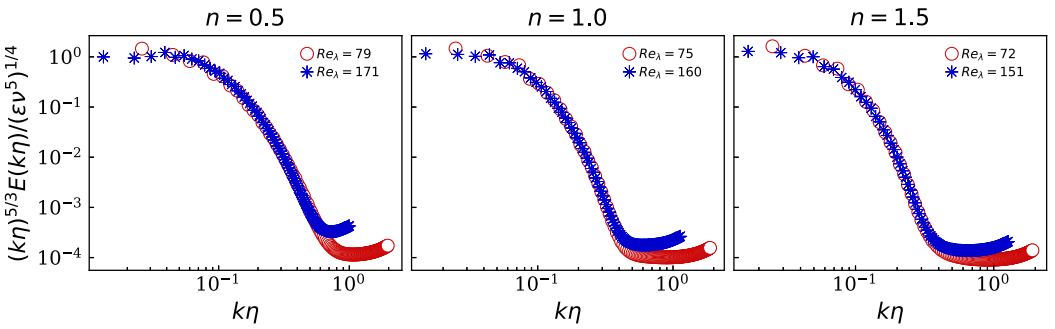

FIG. 2. Energy spectra, multiplied by $k^{5/3}$, each obtained for two values of Re_λ, for (a) $n = 0.5$, (b) $n = 1.0$, and (c) $n = 1.5$. Each spectra is computed by averaging over 20 different snapshots, each separated by 150 turnover times.

numerical mesh of the cubic box for which $\lambda_2 \leqslant \lambda_2^*$, where $\lambda_2^* \leqslant 0$ is a given threshold value. The smaller the prescribed parameter λ_2^*, the smaller is the average volume which encloses the vortex cores in the system. Here only clusters with volume larger than η^3 have been considered as vortices, where $\eta \equiv (\nu^3/\langle\bar{\epsilon_1}\rangle)^{\frac{1}{4}}$ is the Kolmogorov dissipation scale [17] calculated for the Newtonian case ($n = 1$). For all practical purposes, our results show that, by redefining the Kolmogorov scale in a more general way, $\eta_n \equiv (\langle\nu\rangle^3/\langle\bar{\epsilon_n}\rangle)^{1/4}$, the minimum and maximum values obtained among the results for all n were 0.077 for $n = 0.5$ and 0.080 for $n = 1.5$, which are very close to the value obtained for the Newtonian case, $\eta_1 = 0.078$.

Figure 3(a) shows a typical snapshot of the vortex structure at the stationary state of the turbulent flow of a shear-thickening fluid with $n = 1.5$, and calculated for $\lambda_2^* = -10^{-5}$. The contours of λ_2^* (white lines) together with the color maps of the local vorticity and stress computed at the cross section, as highlighted in Fig. 3(a), are shown in Figs. 3(b) and 3(c), respectively. These plots clearly confirm that the λ_2 criterion captures both the intense local vortical motion inside and the high stress outside the vortices.

Despite their chaotic and disordered nature, fully developed turbulent flows can be characterized in terms of certain statistical properties. Here, by identifying distinct vortices over a large number of snapshots of the system, the distribution of vortex sizes, $P(s)$, is computed for a given threshold λ_2^*, where s denotes the volume fraction of a vortex in the system. The results shown in Figs. 4 indicate that, for a fixed value of λ_2^*, the distribution of vortex sizes remains invariant, regardless of the rheological exponent n (within numerical accuracy), which ranges from power-law shear-thinning, $n = 0.25$, to shear-thickening behavior, $n = 1.75$. This is confirmed here by applying the Kolmogorov–Smirnov test [26] to verify if each pair of distributions, for two different values of the rheological exponent n, can be considered as two particular statistical realizations of the same random variable (the null hypothesis). Our results show that the significance levels are smaller than 0.05 in all cases. Consequently, the null hypothesis cannot be rejected, leading to the conclusion that the vortex sizes are indeed likely to be drawn from the same distribution. The fact that rheology has negligible impact on the statistical signature of this turbulent-flow property gives support to the prediction that the structure of Newtonian turbulence at the inertial subrange is robust, meaning that the distribution of vortex sizes is not influenced by the details of the constitutive relation at the microscopic level [13]. We have performed additional simulations at higher values of Reynolds number; namely, $\mathrm{Re}_\lambda = 171$ for a shear-thinning fluid with $n = 0.5$, $\mathrm{Re}_\lambda = 160$ for the Newtonian fluid ($n = 1.0$), and $\mathrm{Re}_\lambda = 151$ for the shear-thickening fluid with $n = 1.5$. The vortex size distributions computed for these cases are shown in the insets of Fig. 4, confirming that the behavior is also valid for higher values of Re_λ.

At this point, we show how fluids possessing very distinct rheological features adapt to display the same vortex size distribution in the fully developed turbulent regime. Energy dissipation is a

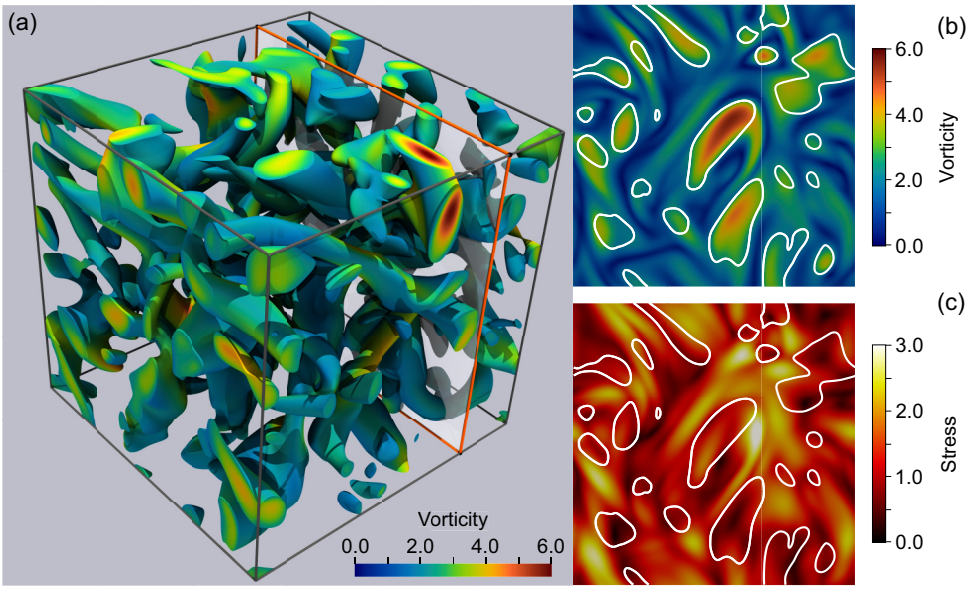

FIG. 3. Vortex identification using the λ_2-*vortex-criterion* [25]. A typical snapshot of the vortex structure at the stationary state of the turbulent flow of a shear-thickening fluid with $n = 1.5$ is shown in panel (a). The isosurfaces are calculated for a threshold value $\lambda_2^* = -10^{-5}$ and the colors correspond to the vorticity amplitude. The highlighted plane in panel (a) indicates the cross section for the color maps in panels (b) and (c) for the vorticity amplitude and stress intensity, respectively. The white lines in panels (b) and (c) are the contours $\lambda_2 = \lambda_2^*$.

key fluctuating quantity in turbulent flows [27] and compared with a purely Newtonian fluid, the non-Newtonian constitutive relation (4) provides an additional degree of freedom, which allows the system to operate with a different characteristic viscosity in the dissipative range, depending on the value of the exponent n. Using again the λ_2-*vortex-criterion* [25] to distinguish regions in space that are inside and outside turbulent eddies, our results show that the energy dissipated per unit mass ϵ, calculated for each cell of the numerical domain, is typically smaller inside the vortices than outside them, regardless of rheology. This general behavior is well exemplified by visualizing a snapshot of the turbulent flow calculated for a shear-thickening fluid, $n = 1.5$, as depicted in the color map of Fig. 5(a). Figure 5(b) shows how the ratio ϵ/ϵ_0 changes with λ_2 for different values of n, where ϵ_0 is rate of energy dissipation per unit of mass for $n = 1$ at $\lambda_2 = 0$. Although all curves display the same qualitative pattern; namely, a slow decrease followed by a minimum at $\lambda_2 \approx 0$, and a comparatively rapid increase for positive values of λ_2, the relative amounts of energy dissipated are strongly dependent on the rheological exponent n.

The global effect of rheology is better visualized when we calculate the ratio ϕ_n between the total energies dissipated outside and inside the vortices,

$$\phi_n = \left\langle \frac{\int_{\lambda_2^*}^{\lambda_2^{\max}} \epsilon(\lambda_2) d\lambda_2}{\int_{\lambda_2^{\min}}^{\lambda_2^*} \epsilon(\lambda_2) d\lambda_2} \right\rangle, \tag{6}$$

where $\lambda_2^{\min}$ and $\lambda_2^{\max}$ are the minimum and maximum values of λ_2 observed during the dynamics, respectively. The integrals are calculated over the entire simulation box, and the average is performed over several snapshots of the turbulent system. In Fig. 5(c) we show the dependence of the ratio ϕ_n/ϕ_1 on n for different values of the threshold λ_2^*. These results reveal that, relative to Newtonian fluids ($n = 1$), shear-thinning fluids ($n<1$) adjust to have an augmented dissipation

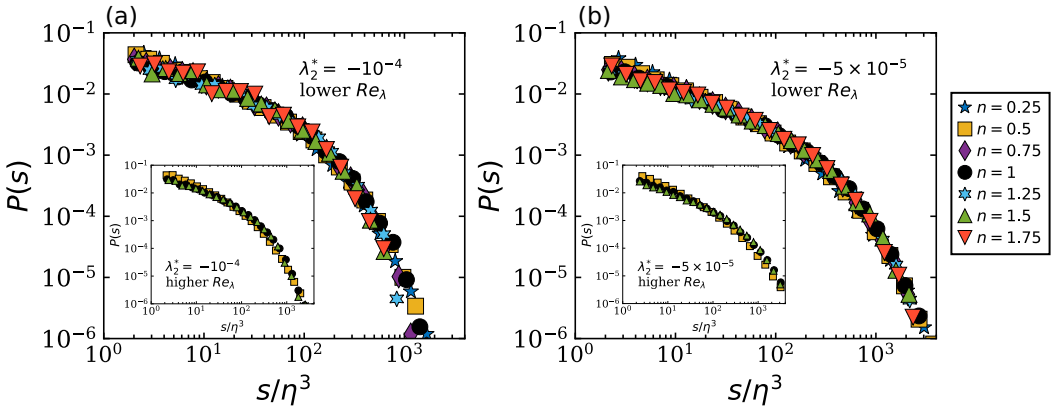

FIG. 4. Vortex size distributions computed for lower Re_λ, for different values of the rheological exponent n, ranging from 0.25 to 1.75, and for two values of the threshold, namely, $\lambda_2^* = -10^{-4}$ (a), and -5×10^{-5} (b). For a given pair of distributions, we applied the Kolmogorov–Smirnov test [26] to verify if they can be considered as two particular statistical realizations of the same random variable (the null hypothesis). For all pairs, the obtained significance levels are smaller than 0.05. Consequently, the null hypothesis cannot be rejected, and we conclude that the vortex sizes are likely to be drawn from the same distribution. The insets show that this behavior is also observed at higher values of Re_λ.

inside the vortices, $\phi_n < \phi_1$, while shear-thickening fluids (n>1) show exactly the opposite behavior, $\phi_n > \phi_1$; namely, they dissipate relatively more outside the vortices. We can therefore argue that non-Newtonian fluids undergoing fully developed turbulence self-organize in distinctive dissipative regimes at the microscopic level so as to display vortex distributions that are statistically identical to that of Newtonian turbulence.

An insightful statistical measure to describe the scaling behavior of fluid turbulence over different spatial scales of the system is the longitudinal structure function [14,28], $S_m^*(\boldsymbol{r}) = \langle\{[\boldsymbol{u}(\boldsymbol{x}+\boldsymbol{r}) - \boldsymbol{u}(\boldsymbol{x})] \cdot \boldsymbol{r}/r\}^m\rangle$, where $\boldsymbol{u}(\boldsymbol{x})$ is the velocity at position $\boldsymbol{x}$, $\boldsymbol{r}$ is the separation vector, $\boldsymbol{r}/r$ its direction unit vector, $r = |\boldsymbol{r}|$, and m is the order. This type of average measure has been extensively used

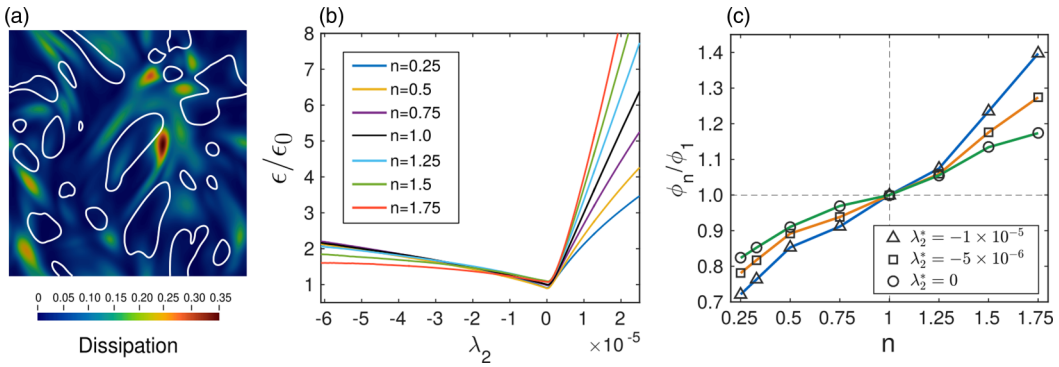

FIG. 5. (a) Energy dissipation rate per unit of mass for the same snapshot and plane highlighted in Fig. 3(a). The white lines correspond to isosurfaces at the threshold value $\lambda_2^* = -10^{-5}$. On average there is more dissipation outside the connected regions with $\lambda_2 < \lambda_2^*$. (b) Spatial and temporal average of the energy dissipation ratio ϵ/ϵ_0 as a function of λ_2 for different values of n, averaged over several eddy-turnover times. (c) The change of the ratio ϕ_n/ϕ_1 as a function of the rheology exponent n for different values of the threshold λ_2^*.

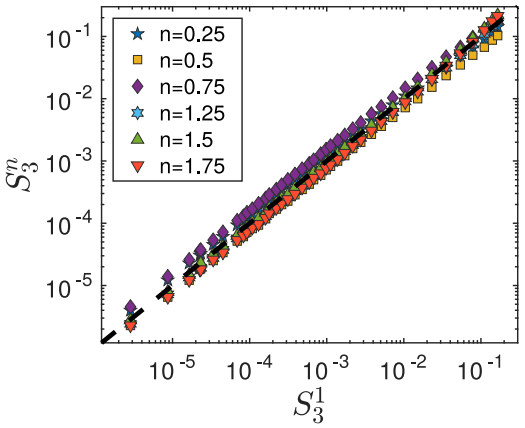

FIG. 6. The scaling relation between S_m^n and S_3 is approximately linear independent of the rheological exponent n, thus rendering the application of ESS for non-Newtonian turbulent flows suitable. The black dashed line represents the 1 : 1 line.

for Newtonian fluids to quantify turbulence from experimental data as well as from numerical simulations across a given inertial-range scale r [29]. The so-called $4/5$ law, which has been derived exactly by Kolmogorov [16] from the Navier–Stokes equations, determines the third-order structure function, $S_3^* = 4/5\langle\epsilon\rangle r$, where $\langle\epsilon\rangle$ is the average rate of energy dissipation per unit mass. Although closed-form expressions for moments of other orders remain unknown, the seminal conceptual framework developed for the K41 theory [15,16] led Kolmogorov to propose a generalized scaling relation for the structure functions; namely, $S_m^*(\boldsymbol{r}) \propto r^{\xi_m^*}$, with the scaling exponents given by $\xi_m^* = m/3$. The fact that the scaling exponents obtained from experiments as well as simulations for Newtonian fluids systematically deviate from this result is broadly accepted nowadays [29] and represents an open and important theoretical challenge in modern turbulence research [30].

In particular, when dealing with fractional and negative moments, it is convenient to use structure functions based on the absolute values of velocity differences rather than of velocity differences [29],

$$S_m(\boldsymbol{r}) = \langle|[\boldsymbol{u}(\boldsymbol{x}+\boldsymbol{r}) - \boldsymbol{u}(\boldsymbol{x})]\cdot \boldsymbol{r}/r|^m\rangle. \tag{7}$$

As in the case of S_m^*, it is known from numerical simulations [29] that these structure functions also obey a scaling relation of the form

$$S_m(\boldsymbol{r}) \propto r^{\xi_m}, \tag{8}$$

although the exponents ξ_m and ξ_m^* may be slightly different [29]. Moreover, we opted to analyze our results by using the extended self-similarity method [31] (ESS), which is known [29] to exhibit larger scaling ranges for Newtonian turbulence than direct logarithmic plots of structure functions versus r. Precisely, the rationale behind the ESS [29] is to obtain the ratio of scaling exponents ξ_m/ξ_3 by plotting the corresponding structure function $S_m(\boldsymbol{r})$ against $S_3(\boldsymbol{r})$, assuming that $\xi_3 = \xi_3^* \equiv 1$. To extend this technique to non-Newtonian turbulence, we first confirm that all third-order structure functions computed from our simulations correlate linearly with the values of $S_3^1(\boldsymbol{r})$ for a Newtonian fluid, thus $S_3^n \sim S_3^1$ (see Fig. 6), where the superscript n characterizes the rheology of the fluid. Considering this linear relation and following the ESS approach, the results of our simulations unequivocally show that the power-law relation, $S_m^n \sim S_3^{\xi_m^n}$, holds for turbulent flows of cross-power-law fluids over more than five orders of magnitude, notwithstanding the order m of the structure function as well as the rheological exponent n. Examples are shown in Fig. 7 for $m = 0.5$, 1.0, and 2.0, and $n = 0.5$, 1.0, and 1.5 and lower and higher values of Re_λ, it is clear from this figure that

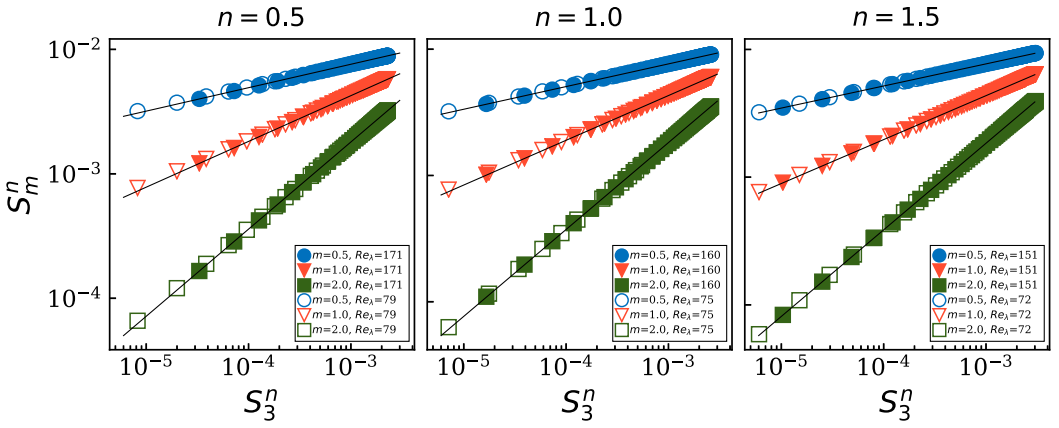

FIG. 7. Extended-self-similarity (ESS) plots for three values of the rheological exponent, $n = 0.5$, 1.0, and 1.5, each showing the respective dependence of the structure functions S_m^n on S_3^n for three different values of the order m and two different values of Re_λ. The black solid lines are the least-squares fits to the simulation data of the power law, $S_m^n \sim S_3^{\xi_m^n}$, where ξ_m^n is the scaling exponent.

the structure functions computed at higher Reynolds numbers have the same scaling exponents ξ_m^n. Figure 8(a) shows the scaling exponents ξ_m obtained from our numerical simulations as a function of the order m for different rheological exponents n.

As already mentioned, it is indisputable from experimental data as well as from extensive numerical simulations that these deviations are indeed present in Newtonian turbulence [29,32–34]. Moreover, taken as a limitation of the scaling result of the K41 theory, which is substantially more evident for higher-order moments, the so-called anomalous scaling phenomenon has been often associated with the need for considering statistical conservation laws in the theoretical framework of hydrodynamic turbulence [30]. Figure 8(b) shows the deviations of the structure function exponents from the K41 theory, $\delta_m^n = (\xi_m^n - m/3)/(m/3)$, as a function of m and for different rheological exponents n. Besides being compatible with the departure from the scaling exponents predicted by the K41 theory for the case of Newtonian turbulence, our results also reveal evidence for a nonuniversal behavior in the deviations of structure functions of non-Newtonian turbulence. More

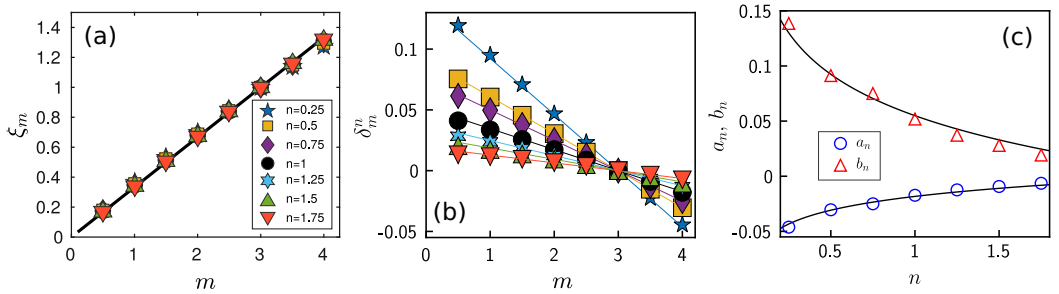

FIG. 8. (a) Dependence of the scaling exponents ξ_m^n of the structure functions on their corresponding order m for different values of the rheological exponent n. The black solid line is the prediction of the K41 theory, $m/3$. (b) Relative deviations of the exponents ξ_m^n from the K41 theory, $\delta_m^n = (\xi_m^n - m/3)/(m/3)$, as a function of the order m, calculated for different rheological exponents n. The solid lines are the linear fits to the data sets, $\delta_m^n = a_n m + b_n$. (c) Dependence of the estimated values of the parameters a_n and b_n on the exponent n. The least-squares fits to these data sets of the functions $a_n = \alpha_1 \ln n + \alpha_2$ and $b_n = \beta_1 \ln n + \beta_2$, dashed lines, gives $\alpha_1 = 0.018 \pm 0.001$, $\alpha_2 = -0.018 \pm 0.001$, $\beta_1 = -0.054 \pm 0.004$, and $\beta_2 = 0.055 \pm 0.003$.

precisely, all deviations δ_m^n decrease monotonically with m, being practically zero for $m = 3$, positive for $m<3$, and negative for $m>3$. Moreover, for any fixed value of $m \neq 0$, the absolute values of δ_m^n decrease systematically with the rheological exponent n. As also shown in Fig. 8(b), the linear fits performed to all data sets show that the exponent deviations δ_m^n follow closely the relation $\delta_m^n = a_n m + b_n$, with $r^2>0.994$ for any value of the rheological exponent n. The estimated values of the parameters a_n and b_n are shown as functions of n in Fig. 8(c). The least-squares fits to these data sets of the functions $a_n = \alpha_1 \ln n + \alpha_2$ and $b_n = \beta_1 \ln n + \beta_2$ gives $\alpha_1 = 0.018 \pm 0.001$, $\alpha_2 = -0.018 \pm 0.001$, $\beta_1 = -0.054 \pm 0.004$, and $\beta_2 = 0.055 \pm 0.003$. As depicted, the agreement between numerical data and fitting relations is excellent in both cases.

IV. CONCLUSIONS

In conclusion, we disclosed a self-organized mechanism of non-Newtonian turbulence through which the particular rheology of the fluid adjusts to comply with the statistical invariance found for the vortex size distribution. We also revealed a systematic dependence on the rheology of the anomalous scaling observed in the deviations from the K41 theory.

ACKNOWLEDGMENTS

We thank the Brazilian agencies CNPq, CAPES, FUNCAP, and the National Institute of Science and Technology for Complex Systems for financial support.

[1] D. N. Ku, Blood flow in arteries, Annu. Rev. Fluid Mech. **29**, 399 (1997).
[2] C. Vlachopoulos, M. O'Rourke, and W. N. Wilmer, *McDonald's Blood Flow in Arteries: Theoretical, Experimental, and Clinical Principles* (CRC Press, London, 2011).
[3] R. W. Hanks and B. H. Dadia, Theoretical analysis of the turbulent flow of non-Newtonian slurries in pipes, AIChE J. **17**, 554 (1971).
[4] F. Forrest and G. A. Grierson, Friction losses in cast iron pipe carrying paper stock, Paper Trade J. **92**, 39 (1931).
[5] B. A. Toms, Some observations on the flow of linear polymer solutions through straight tubes at large Reynolds numbers, in *Proceedings of the First International Congress on Rheology* (North Holland, Amsterdam, 1948), Vol. 2, pp. 135–141.
[6] D. W. Dodge and A. B. Metzner, Turbulent flow of non-Newtonian systems, AIChE J. **5**, 189 (1959).
[7] D. Samanta, Y. Dubief, M. Holzner, C. Schäfer, A. N. Morozov, C. Wagner, and B. Hof, Elasto-inertial turbulence, Proc. Natl. Acad. Sci. USA **110**, 10557 (2013).
[8] G. H. Choueiri, J. M. Lopez, and B. Hof, Exceeding the Asymptotic Limit of Polymer Drag Reduction, Phys. Rev. Lett. **120**, 124501 (2018).
[9] A. Acrivos, M. J. Shah, and E. E. Petersen, Momentum and heat transfer in laminar boundary-layer flows of non-Newtonian fluids past external surfaces, AIChE J. **6**, 312 (1960).
[10] G. Gioia and P. Chakraborty, Spectral derivation of the classic laws of wall-bounded turbulent flows, Proc. R. Soc. London, Ser. A **473**, 20170354 (2017).
[11] J. Singh, M. Rudman, and H. M. Blackburn, The effect of yield stress on pipe flow turbulence for generalised Newtonian fluids, J. Non-Newtonian Fluid Mech. **249**, 53 (2017).
[12] E. De Angelis, C. M. Casciola, R. Benzi, and R. Piva, Homogeneous isotropic turbulence in dilute polymers, J. Fluid Mech. **531**, 1 (2005).
[13] A. A. Townsend, *The Structure of Turbulent Shear Flow*, 2nd ed. (Cambridge University Press, Cambridge, 1980).
[14] G. I. Taylor, Statistical theory of turbulence, Proc. R. Soc. London, A **151**, 421 (1935).

[15] A. N. Kolmogorov, The local structure of turbulence in incompressible viscous fluid for very large Reynolds numbers, Dokl. Akad. Nauk SSSR **30**, 301 (1941).
[16] A. N. Kolmogorov, Dissipation of energy in locally isotropic turbulence, Dokl. Akad. Nauk SSSR **32**, 16 (1941).
[17] Uriel Frisch, *Turbulence: The Legacy of A. N. Kolmogorov* (Cambridge University Press, Minneapolis, 1995).
[18] T. S. Lundgren, Linearly Forces Isotropic Turbulence, Tech. Rep. (University of Minnesota, Minneapolis, 2003).
[19] C. Rosales and C. Meneveau, Linear forcing in numerical simulations of isotropic turbulence: Physical space implementations and convergence properties, Phys. Fluids **17**, 095106 (2005).
[20] S. Popinet, Gerris: A tree-based adaptive solver for the incompressible Euler equations in complex geometries, J. Comput. Phys. **190**, 572 (2003).
[21] The adaptively refined results obtained from the code GERRIS are compared with a standard Newtonian spectral DNS code at the link: http://gfs.sourceforge.net/examples/examples/forcedturbulence.html.
[22] T. Dombre, U. Frisch, J. M. Greene, M. Hénon, A. Mehr, and A. M. Soward, Chaotic streamlines in the ABC flows, J. Fluid Mech. **167**, 353 (1986).
[23] K. R. Sreenivasan, The energy dissipation in turbulent shear flows, in *Synposium on Developments in Fluid Dynamics and Aerospace Engineering*, edited by S. M. Deshpande, A. Prahu, K. R. Sreenivasan, and P. R. Viswanath (Interline Publishers, Bangalore, 1995), pp. 159–190.
[24] A. S. Monin and A. M. Yaglom, *Statistical Fluid Mechanics, Volume II: Mechanics of Turbulence (Dover Books on Physics)* (Dover Publications, Mineola, 2007).
[25] J. Jeong and F. Hussain, On the identification of a vortex, J. Fluid Mech. **285**, 69 (1995).
[26] Frederick James, *Statistical Methods in Experimental Physics* (World Scientific Publishing Company, London, 2006).
[27] P. K. Yeung, X. M. Zhai, and K. R. Sreenivasan, Extreme events in computational turbulence, Proc. Natl. Acad. Sci. USA **112**, 12633 (2015).
[28] J. Schumacher, J. D. Scheel, D. Krasnov, D. A. Donzis, V. Yakhot, and K. R. Sreenivasan, Small-scale universality in fluid turbulence, Proc. Natl. Acad. Sci. USA **111**, 10961 (2014).
[29] S. Y. Chen, B. Dhruva, S. Kurien, K. R. Sreenivasan, and M. A. Taylor, Anomalous scaling of low-order structure functions of turbulent velocity, J. Fluid Mech. **533**, 183 (2005).
[30] G. Falkovich and K. R. Sreenivasan, Lessons from hydrodynamic turbulence, Phys. Today **59**(4), 43 (2006).
[31] R. Benzi, S. Ciliberto, R. Tripiccione, C. Baudet, F. Massaioli, and S. Succi, Extended self-similarity in turbulent flows, Phys. Rev. E **48**, R29 (1993).
[32] C. Meneveau and K. R. Sreenivasan, Simple Multifractal Cascade Model for Fully Developed Turbulence, Phys. Rev. Lett. **59**, 1424 (1987).
[33] S. Kurien and K. R. Sreenivasan, Dynamical equations for high-order structure functions, and a comparison of a mean-field theory with experiments in three-dimensional turbulence, Phys. Rev. E **64**, 056302 (2001).
[34] V. Yakhot, Mean-field approximation and a small parameter in turbulence theory, Phys. Rev. E **63**, 026307 (2001).